AN ADAPTIVE OPTIMAL-KERNEL TIME-FREQUENCY REPRESENTATION

Douglas L. Jones[◇] *and Richard G. Baraniuk*[□ *]

[◇] Coordinated Science Laboratory
University of Illinois
1308 West Main Street
Urbana, IL 61801
E-mail: d-jones@csl.uiuc.edu

[□] Department of Electrical and Computer Engineering
Rice University
P.O. Box 1892, Houston, TX 77251–1892
E-mail: richb@rice.edu

Submitted to *IEEE Transactions on Signal Processing*
Submitted: August 1992, Revised: January 1995

Abstract

Time-frequency representations with fixed windows or kernels figure prominently in many applications, but perform well only for limited classes of signals. Representations with signal-dependent kernels can overcome this limitation. However, while they often perform well, most existing schemes are block-oriented techniques unsuitable for on-line implementation or for tracking signal components with characteristics that change with time. The time-frequency representation developed here, based on a signal-dependent radially Gaussian kernel that adapts over time, overcomes these limitations. The method employs a short-time ambiguity function both for kernel optimization and as an intermediate step in computing constant-time slices of the representation. Careful algorithm design provides reasonably efficient computation and allows on-line implementation. Certain enhancements, such as cone-kernel constraints and approximate retention of marginals, are easily incorporated with little additional computation. While somewhat more expensive than fixed-kernel representations, this new technique often provides much better performance. Several examples illustrate its behavior on synthetic and real-world signals.

*Sponsored by the National Science Foundation, grant nos. MIP 9012747 and MIP 9457438, the Joint Services Electronics Program, grant no. N00014-90-J-1270, the Texas Advanced Technology Program, grant no. TX-ATP 003604–002, and the Sound Group of the Computer-based Education Research Laboratory at the University of Illinois.

1 Introduction

Time-frequency representations (TFRs) are a central signal analysis tool in a wide variety of applications. A large number of bilinear TFRs have been proposed, each differing only in the choice of a kernel function [1]. Each distribution in Cohen's bilinear class can be interpreted as the two-dimensional Fourier transform of a weighted version of the ambiguity function (AF) of the signal to be analyzed. That is, if $P(t, \omega)$ is a bilinear TFR, then[1]

$$P(t, \omega) \;=\; \frac{1}{4\pi^2} \iint A(\theta, \tau)\, \Phi(\theta, \tau)\, e^{-j\theta t - j\tau\omega}\, d\theta\, d\tau. \tag{1}$$

$A(\theta, \tau)$ is called the symmetrical AF and is given by

$$A(\theta, \tau) \;\equiv\; \int s\left(t + \frac{\tau}{2}\right) s^*\left(t - \frac{\tau}{2}\right) e^{j\theta t}\, dt. \tag{2}$$

Different choices for the kernel function Φ yield widely different TFRs. Several particular choices are illustrated in Figure 1 for a test signal consisting of several impulses, two simultaneous sinusoids, a Gaussian pulse, and two parallel linear chirps.[2] Figures 1(a)–(d) contain equal energy contour plots of the Wigner distribution, spectrogram (squared magnitude of the short-time Fourier transform), Choi-Williams distribution [2], and cone-kernel representation [3], respectively. While in each case the parameters were chosen to result in the most visually appealing representation, each of these TFRs exhibits either interference components, amplitude variations, or excessive broadening.

In recent years, it has become apparent that no single kernel can give adequate performance for a large class of signals; hence, there has been increasing interest in signal-dependent or adaptive TFRs, in which the kernel function varies with the signal. Arguments for signal dependence and surveys of the related literature can be found in [4, 5].

A number of signal-dependent TFRs have been developed. Among the most promising are those based on optimality criteria, including a signal-dependent TFR based on radially Gaussian kernels [6–8].[3] The algorithm computes the AF of the entire signal, determines the optimal kernel $\Phi_{\mathrm{opt}}(\theta, \tau)$ based on that AF, and obtains the optimal TFR via Fourier transformation according to (1). This representation performs well for a wide variety of signals, is fully automatic, and has a computational complexity on the same order as fixed-kernel methods. Figure 1(e) illustrates this optimal-kernel TFR for the multicomponent test signal.

The signal-dependent representation performs much better than the fixed-kernel methods in Figure 1; however, it is limited to processing relatively short signals in an off-line fashion. Moreover, this block-oriented technique designs only one kernel for the entire signal, thus forcing compromises in the kernel design for signals with multiple components. The TFR of Figure 1(e) still contains visible low-level cross-component artifacts and some distortion of certain signal components.

[1] All integrals run from $-\infty$ to ∞ unless otherwise noted.
[2] See (40) in Appendix A for the formula for this signal.
[3] An alternative optimal TFR based on binary masking kernels is developed in [5, 9].

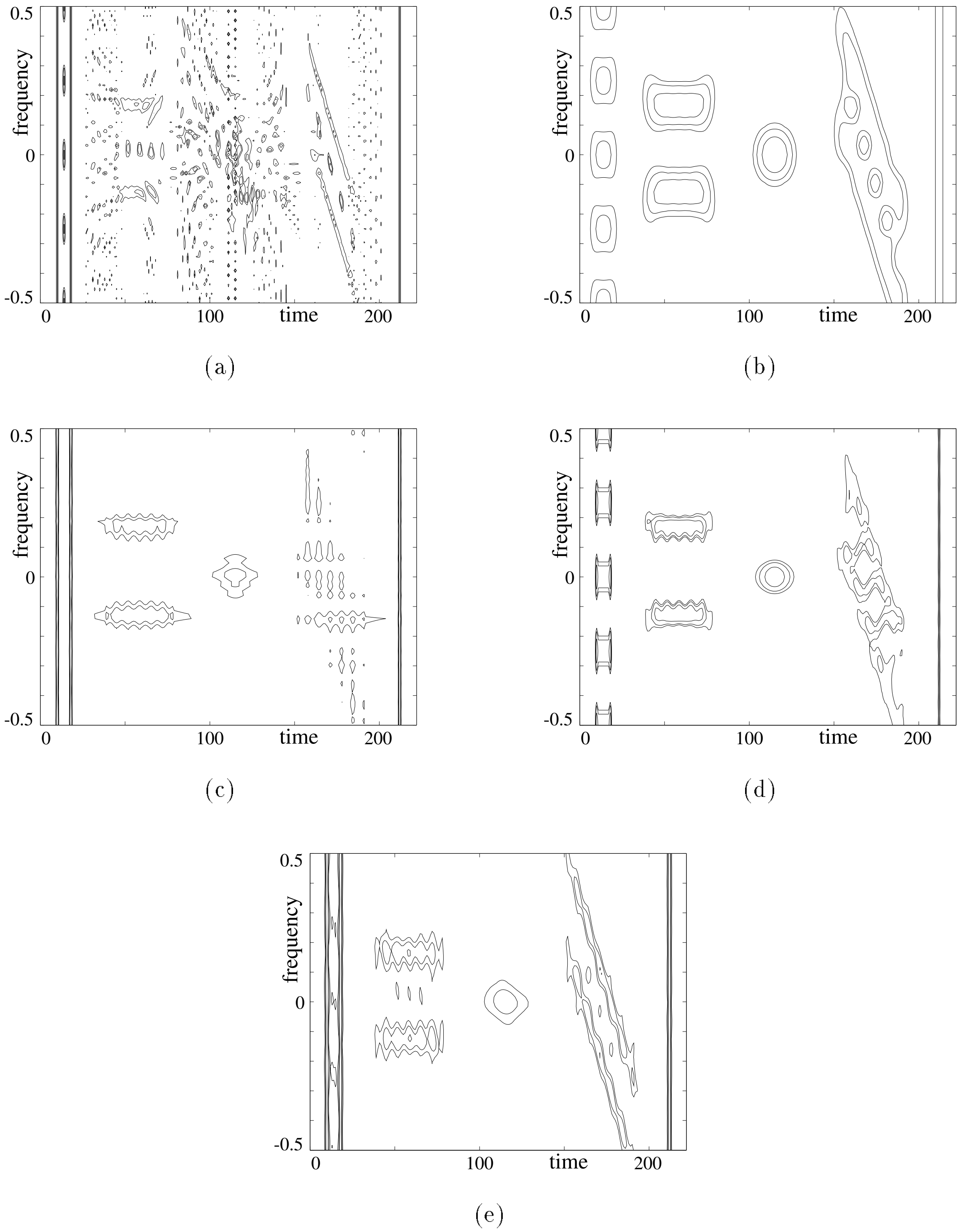

Figure 1: *Comparison of several state-of-the-art TFRs of the synthetic test signal (40) from Appendix A. (a) Wigner distribution. (b) Spectrogram computed with a 27-point Gaussian window. (c) Choi-Williams distribution with smoothing parameter* $\sigma = 1$ *[2]. (d) Cone-kernel representation with* τ*-extent parameter* $= 33$ *[3]. (e) Radially Gaussian optimal-kernel TFR computed using volume* $\alpha = 2$ *[6–8].*

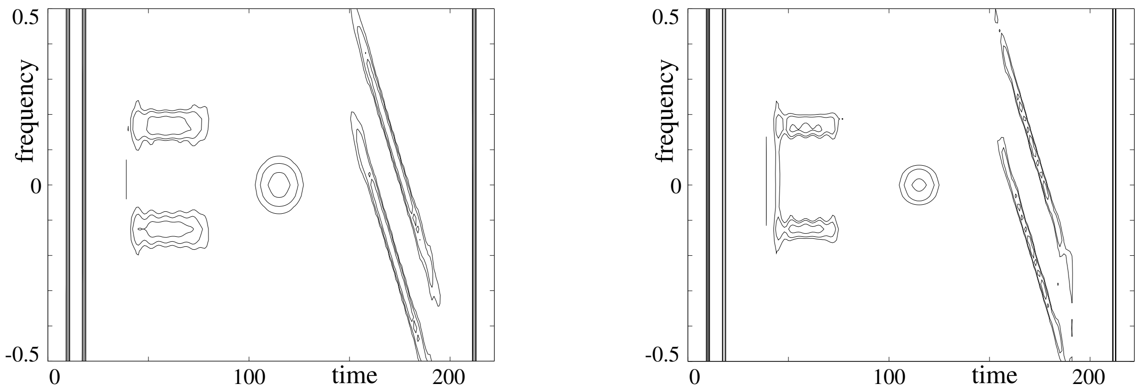

(a) (b)

Figure 2: *New adaptive TFRs of the synthetic test signal (40) from Appendix A. (a) Adaptive optimal-kernel (AOK) TFR computed using volume $\alpha = 1.4$, window width $2T = 32$, and one kernel optimization iteration per input time sample. (The AOK TFR is quite insensitive to these values.) (b) AOK TFR with additional time-support (cone) constraint (see Section 6.2).*

Adaptation of the kernel over time is beneficial, because it permits the kernel to match the local signal characteristics [4]. An ambiguity-domain based design procedure like the radially Gaussian kernel optimization technique mentioned above does not immediately admit such time localization, because each point in the AF includes information from all times and frequencies in the signal (see (2)). In this paper, we surmount this difficulty by developing a time-localized, *short-time ambiguity function* (STAF) $A(t;\, \theta, \tau)$ [10, 11]. Application of the radially Gaussian kernel optimization procedure of [6–8] to the STAF localized at time t produces a localized optimal kernel $\Phi_{\mathrm{opt}}(t;\, \theta, \tau)$ and a time-frequency distribution slice at time t. Figure 2 shows two adaptive optimal-kernel (AOK) TFRs for the same multicomponent test signal used in Figure 1. These TFRs adapt their kernels to each set of signal components, and highly concentrated, readable representations result.

After a review of radially Gaussian optimal-kernel TFRs in Section 2, we derive the running-time adaptive algorithm in Section 3 and consider its efficient implementation in Section 4. Further examples follow in Section 5. Performance-enhancing extensions to the technique are considered in Section 6, including appending extra constraints to satisfy approximate marginal distributions and to preserve signal time support. We close in Section 7 with a discussion and conclusions.

2 Radially Gaussian Kernels

The signal-dependent TFR proposed in [6–8] is based on kernels with Gaussian radial cross-sections

$$\Phi(\theta, \tau) \;=\; \exp\left(-\frac{\theta^2 + \tau^2}{2\sigma^2(\psi)}\right). \tag{3}$$

The function $\sigma(\psi)$ controls the spread of the Gaussian at radial angle ψ; we will call $\sigma(\psi)$ the *spread function.* Clearly, if σ is smooth, then Φ is also smooth. The angle ψ is measured between the radial line through the point (θ, τ) and the θ axis

$$\psi \equiv \arctan \frac{\tau}{\theta}. \tag{4}$$

It is natural to express radially Gaussian kernels in polar coordinates;[4] using $r = \sqrt{\theta^2 + \tau^2}$ as the radius variable,

$$\Phi(r, \psi) \;=\; \exp\left(-\frac{r^2}{2\sigma^2(\psi)}\right). \tag{5}$$

A high quality time-frequency representation results when the kernel is well matched to the components of a given signal. The radially Gaussian kernel is adapted to a signal by solving the following optimization problem:

$$\max_{\Phi} \int_0^{2\pi} \int_0^{\infty} |A(r, \psi)\, \Phi(r, \psi)|^2\, r\, dr\, d\psi \tag{6}$$

subject to

$$\Phi(r, \psi) \;=\; \exp\left(-\frac{r^2}{2\sigma^2(\psi)}\right) \tag{7}$$

$$\frac{1}{4\pi^2} \int_0^{2\pi} \int_0^{\infty} |\Phi(r, \psi)|^2\, r\, dr\, d\psi \;=\; \frac{1}{4\pi^2} \int_0^{2\pi} \sigma^2(\psi)\, d\psi \;\le\; \alpha, \qquad \alpha \ge 0. \tag{8}$$

Here, $A(r, \psi)$ is the AF of the signal in polar coordinates. We denote the solution to the above optimization problem by Φ_{opt}. The AF is utilized in the optimization formulation because of its important separation property: the auto- and cross-components separate somewhat in the AF plane, with the auto-components lying centered at the origin and the cross-components lying away from the origin [12].

The constraints and performance index are motivated by a desire to suppress cross-components and to pass auto-components with as little distortion as possible. The first constraint (7) limits the scope of the optimization to the class of radially-Gaussian kernels. Thus, the kernel is constrained to be a lowpass filter. Since the AF auto-components are centered at the origin, this encourages the kernel to preferentially pass auto-components. The second constraint (8) limits the volume of the kernel to α, so that cross-components are suppressed. An advantage of this formulation is that the constraints are insensitive to both the time-scale and orientation of the signal in time-frequency.

The performance measure (6) determines the shape of the passband of the optimal radially Gaussian kernel; it expresses a desire to minimize auto-component distortion by passing as much auto-component energy as possible into the TFR for a kernel of fixed volume. Clearly, in order to maximize the performance measure, $\Phi(r, \psi)$ should be large where $A(r, \psi)$ is large, regardless of whether the peaks correspond to auto- or cross-components. However, the radially Gaussian

[4]In the sequel, (θ, τ) will represent the ambiguity plane in rectangular coordinates, while (r, ψ) will represent this plane in polar coordinates.

constraint favors kernels that pass components concentrated at the origin, which are the auto-components, because a large spread in the direction of cross-components requires excessive kernel volume.

By controlling the volume under the optimal kernel, the parameter α controls the tradeoff between cross-component suppression and smearing of the auto-components. If α is too small, then the kernel will induce excessive smearing of the auto-components. If α is too large, then extra kernel volume will be available to extend over the cross-components, and little cross-component suppression will result. While the exact value of kernel volume is application-specific, we have found $1 \leq \alpha \leq 5$ to be reasonable bounds [7,8].

The shape of a radially Gaussian kernel is completely parameterized by the spread function $\sigma(\psi)$, so finding the optimal, radially-Gaussian kernel Φ_{opt} for a signal is equivalent to finding the optimal function $\sigma_{\text{opt}}(\psi)$ for the signal.

Signal analysis using the optimal radially Gaussian kernel TFR proceeds as follows. First, the AF of the signal is computed. Next, the optimization problem (6)–(8) is solved for the optimal kernel. A simple iterative procedure can be utilized to efficiently solve the problem in $O(IM^2)$ computations, where M is the number of frequency samples in the optimal-kernel TFR and I is the number of iterations (typically less than 30) [7,8]. More details are given in Section 4.3. Finally, the optimal-kernel TFR is computed as the two-dimensional Fourier transform of the product of the AF and the optimal kernel, as in (1).

3 A Running-Time Algorithm

The signal-dependent TFR with radially Gaussian kernel described in Section 2 has many attractive qualities, but it is based on a block algorithm that designs only one kernel for the entire signal. For signals with characteristics that change over time, for real-time, on-line operation, or for very long signals, an *adaptive* signal-dependent TFR is more desirable. An adaptive algorithm alters the kernel at each time to achieve optimal local performance, thus better tracking the changes in a signal.

The AF integrates information from all time and frequency locations, so a time-adaptive algorithm must include a means of localizing the AF content to a relatively short interval of time surrounding the current time, t. In this section, we define a time-localized *short-time ambiguity function* (STAF) and combine it with the radially Gaussian kernel optimization procedure to produce a time-adaptive kernel optimized for each individual time-frequency distribution slice at time t [10,11].

We define the *symmetrical* STAF $A(t;\,\theta,\tau)$ as the AF of a windowed signal, with the window centered at time t. Defining the instantaneous correlation of a signal $s(t)$ as

$$R(t,\tau) \;\equiv\; s^*\left(t-\frac{\tau}{2}\right) s\left(t+\frac{\tau}{2}\right), \tag{9}$$

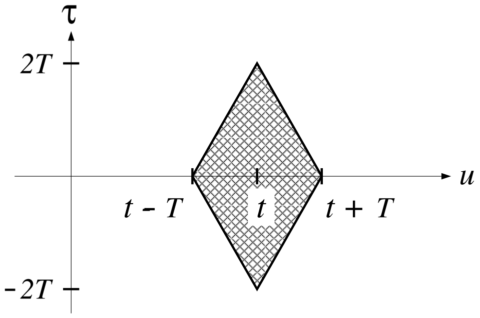

Figure 3: *The samples of the instantaneous correlation function in the (u, τ) plane included in the STAF at time t.*

the STAF is given by

$$\begin{aligned} A(t;\,\theta,\tau) &= \int R(u,\tau)\, w^*\left(u - t - \frac{\tau}{2}\right) w\left(u - t + \frac{\tau}{2}\right) e^{j\theta u}\, du \\ &= \int s^*\left(u - \frac{\tau}{2}\right) w^*\left(u - t - \frac{\tau}{2}\right) s\left(u + \frac{\tau}{2}\right) w\left(u - t + \frac{\tau}{2}\right) e^{j\theta u}\, du, \end{aligned} \qquad (10)$$

where $w(u)$ is a symmetrical window function equal to zero for $|u| > T$. The variables τ and θ are the usual ambiguity plane parameters; the variable t indicates the center position of the signal window. Figure 3 illustrates the region of support of the windowed instantaneous correlation function in the (u, τ) plane. Only the portion of the signal in the interval $[t - T,\ t + T]$ is incorporated into $A(t;\,\theta,\tau)$, and the range of τ for which the windowed instantaneous correlation function is nonzero is $|\tau| < 2T$.

Given a time-localized STAF, the adaptive signal-dependent TFR with radially Gaussian kernel is straightforward to define. Conceptually, the algorithm proceeds as follows. At each time t, we compute the STAF centered at time t in both rectangular and polar coordinates and solve the optimization problem (6)–(8) to obtain the optimal kernel $\Phi_{\rm opt}(t;\,\theta,\tau)$. Since the STAF varies with time, so does the optimal signal-dependent kernel. Once the optimal kernel has been determined, a single, current-time slice of the adaptive optimal-kernel (AOK) TFR is computed as one slice (at time t only) of the two-dimensional Fourier transform of the STAF-kernel product:

$$P_{\rm AOK}(t,\omega) = \frac{1}{4\pi^2} \iint A(t;\,\theta,\tau)\, \Phi_{\rm opt}(t;\,\theta,\tau)\, e^{-j\theta t - j\tau\omega}\, d\theta\, d\tau. \qquad (11)$$

The AOK procedure for discrete-time data is defined similarly.

4 Fast Implementation

Although straightforward conceptually, direct implementation of the AOK procedure described above would be quite expensive computationally, requiring $O(M^2 \log M)$ operations per output time slice for M samples in the STAF window. Fortunately, a number of tricks can be applied to greatly reduce the arithmetic required to implement this algorithm. The three expensive components are the computation of the STAF, the optimal-kernel, and the constant-time slice of the AOK TFR. We now describe techniques to reduce the cost of each of these procedures to a total cost of $O(M^2)$ computations per signal sample.

4.1 STAF computation in rectangular coordinates

Fast implementation of the STAF depends on an *asymmetrical* form of the AF, for three reasons: (1) it supports a causal implementation suitable for on-line computation, (2) it admits a computationally efficient recursive implementation, and (3) it allows full-rate sampling in the correlation lag (τ) variable, which provides an alias-free distribution for signals sampled at or above the Nyquist rate.

Recursive computation of the STAF greatly reduces the computational burden. We begin by defining an asymmetrical STAF that is amenable to recursive computation:

$$\begin{aligned}\widetilde{A}(t;\,\theta,\tau) \;\;\equiv\;\; & \int s^*(t+T-v-\tau)\; w^*(-v+T-\tau) \\ & \qquad\qquad \cdot\, s(t+T-v)\; w(-v+T)\; e^{-j\theta v}\, dv. \end{aligned} \tag{12}$$

By making the change of variables $u = t + T - \tau/2 - v$ in (10), the relationship between the symmetrical and the asymmetrical STAFs can be shown to be

$$A(t;\,\theta,\tau) \;=\; e^{j\theta(T-t-\tau/2)}\, \widetilde{A}(t;\,\theta,\tau). \tag{13}$$

Considering the special case of rectangular windows (which will be assumed for the remainder of the paper; fast algorithms can also be derived for certain other recursively computable windows), and defining the "current sample time" as $t_s = t + T$, (12) reduces to

$$\widetilde{A}(t_s - T;\,\theta,\tau) \;=\; \int_0^{2T-\tau} s^*(t_s - v - \tau)\; s(t_s - v)\; e^{-j\theta v}\, dv, \qquad \tau \geq 0. \tag{14}$$

In practice, actual computation of the asymmetrical STAF requires discretization. Without loss of generality, assume that the signal is bandlimited to frequencies strictly less than π rad/sec and is sampled at a rate of one sample per second. Then, a discrete approximation to the asymmetrical STAF, with $n_s = n + T$, is

$$\widetilde{A}_{\mathrm{d}}(n_s - T;\,\theta,k) \;=\; \sum_{p=0}^{2T-k-1} s^*\left(n_s - p - k\right)\, s\left(n_s - p\right)\, e^{-j\theta p}. \tag{15}$$

For a given θ and k, the sum in (15) simply represents convolution with a causal FIR filter having impulse response $h(p) = e^{-j\theta p}$, $p = 0, 1, \ldots, 2T - k - 1$. This generalized comb filter can be efficiently realized using the recursion

$$\begin{aligned}\widetilde{A}_{\mathrm{d}}(n_s - T;\,\theta,k) \;\;=\;\; & e^{-j\theta}\,\widetilde{A}_{\mathrm{d}}(n_s - 1;\theta,k) \;+\; s(n_s)\,s^*(n_s - k) \\ & -\, e^{-j\theta(2T-k)}\, s(n_s - (2T-k))\, s^*(n_s - k - (2T-k)), \end{aligned} \tag{16}$$

which is nothing more than a "running" or recursive discrete Fourier transform update [13, pp. 106–108] of the discretized, asymmetrical instantaneous correlation function

$$\tilde{R}_{\mathrm{d}}(n_s, k) \;\equiv\; s(n_s)\, s^*(n_s - k). \tag{17}$$

Unser [14] and Amin [15–18] have utilized similar recursions in fixed window/kernel time-frequency analysis. In practice, a stable algorithm is desired, so the following recursion is actually implemented

$$\begin{aligned} \tilde{A}_{\mathrm{d}}(n_s - T;\, \theta, k) \;&=\; \beta\, e^{-j\theta}\, \tilde{A}_{\mathrm{d}}(n_s - 1; \theta, k) \;+\; s(n_s)\, s^*(n_s - k) \;-\; \beta^{2T-k}\, e^{-j\theta(2T-k)} \\ &\qquad \cdot s(n_s - (2T - k))\, s^*(n_s - k - (2T - k)) \\ &=\; \beta\, e^{-j\theta}\, \tilde{A}_{\mathrm{d}}(n_s - 1; \theta, k) \;+\; \tilde{R}_{\mathrm{d}}(n_s, k) \;-\; \beta^{2T-k}\, e^{-j\theta(2T-k)} \\ &\qquad \cdot \tilde{R}_{\mathrm{d}}(n_s - (2T - k),\, k), \end{aligned} \tag{18}$$

where β is a positive real number just less than one. A discrete version of the symmetrical STAF is obtained from (13) as

$$A_{\mathrm{d}}(n;\, \theta, k) \;=\; e^{j\theta(T+n-k/2)}\, \tilde{A}_{\mathrm{d}}(n + T;\, \theta, k). \tag{19}$$

Obtaining the discretized symmetrical STAF via the asymmetrical STAF yields great computational benefits due to the recursive updating. Samples of the discrete instantaneous asymmetrical correlation function can be computed only once and then reused extensively, thus making the cost per each STAF sample point according to (18) only two complex multiplications and two complex additions. For M samples in both θ and τ (the usual arrangement), the total cost of computing the STAF is thus $O(M^2)$ per input sample point, as opposed to the $O(M^2 \log M)$ cost of computing the STAF from scratch at each output sample time. An additional benefit of this scheme is that half-sample lags are avoided, thus preventing the need for interpolation or oversampling to obtain an unaliased TFR [19–22] (see Appendix B).

Finally, note that only STAF samples corresponding to positive lags τ need be computed or stored, because negative lag values can be obtained from the positive lags using the symmetry relation

$$A(t;\, \theta, \tau) \;=\; A^*(t;\, -\theta, -\tau), \tag{20}$$

with equivalent expressions for discretized STAFs.

4.2 STAF computation in polar coordinates

Optimization of the radially Gaussian kernel requires samples of the squared magnitude of the STAF on a polar grid. Define the polar sampled STAF as

$$A_{\mathrm{p}}(n;\, b, q) \;\equiv\; A(n;\, r, \psi)|_{r=b\Delta_r,\ \psi=q\Delta_\psi} \;=\; A(n;\, \theta, \tau)|_{\theta=b\Delta_r \cos q\Delta_\psi,\ \tau=b\Delta_r \sin q\Delta_\psi},$$

$$b \;=\; 0, 1, \ldots, B-1, \qquad q \;=\; 0, 1, \ldots, Q-1, \tag{21}$$

with Δ_r and Δ_ψ the radius and angle step sizes, respectively. Samples of the STAF at arbitrary sample points in θ and τ can be computed efficiently using the recursion (18). The only complication is that the lagged signal samples no longer fall on integer sample points, and thus computation of the appropriate instantaneous correlation function values incurs the additional cost of interpolating the signal samples.

An alternative, less expensive approach interpolates polar samples of the squared magnitude of the STAF from the squared magnitude of the rectangularly sampled STAF. Bilinear interpolation works quite well in practice: the four rectangular sample points surrounding the polar sample point are used to linearly interpolate in the θ direction along the sides of the rectangle, and then linearly interpolate in the τ direction to the desired point. The cost is only three real multiplications and three real additions per polar sample point. We have noticed slight differences between the results obtained using the exact polar STAF computation and the rectangular STAF interpolation, but they appear insignificant and are generally outweighed by the computational advantages of the interpolation-based approach.

4.3 Kernel optimization

To compute the adaptive optimal kernel at time t, we first discretize the optimization problem (6)–(8), with the AF $A(r,\psi)$ replaced by the discrete, polar-coordinate STAF $A_{\mathrm{p}}(n;b,q)$ from (21) and the radially Gaussian kernel $\Phi(r,\psi)$ replaced by the short-time discrete polar kernel

$$\Phi_{\mathrm{p}}(n;b,q) \;\equiv\; \exp\left(-\frac{b^2\Delta_r^2}{2\sigma_q^2}\right). \tag{22}$$

This discrete radially Gaussian kernel is parameterized by a *spread vector* $\underline{\sigma}$, whose components σ_q correspond to samples of the continuous-variable spread function

$$\sigma_q \;=\; \sigma(q\Delta_\psi), \qquad q=0,1,\ldots,Q-1. \tag{23}$$

The optimal spread vector $\underline{\sigma}_{\mathrm{opt}}$ for a signal is defined as the solution to the discretized version of (6)–(8), and can be computed using the iterative *step-project algorithm* developed in [6–8]. Denote the estimate of the optimal spread vector at iteration i by $\underline{\sigma}(i)$. Then, the step-project algorithm takes the form

$$\begin{aligned} \text{Step}: \qquad \underline{\tilde{\sigma}}(i) \;&=\; \underline{\sigma}(i) \;+\; \mu(i)\,\underline{\nabla} f(i) \\ \text{Project}: \qquad \underline{\sigma}(i+1) \;&=\; \underline{\tilde{\sigma}}(i)\,\frac{\gamma}{\|\underline{\tilde{\sigma}}(i)\|}. \end{aligned}$$

Here, $\mu(i)>0$ is the step size, $\gamma \equiv (4\pi^2\alpha/\Delta_\psi)^{1/2}$, $\|\underline{\tilde{\sigma}}(i)\|$ is the usual Euclidean norm of $\tilde{\sigma}(i)$, and $\underline{\nabla} f(i)$ is the gradient of the discretized version of the performance measure (6) evaluated at the spread vector $\underline{\sigma}(i)$

$$\underline{\nabla} f(i) \;\equiv\; \left[\frac{\partial f}{\partial\sigma_0(i)},\;\ldots\;,\frac{\partial f}{\partial\sigma_{Q-1}(i)}\right]^T, \tag{24}$$

$$\frac{\partial f}{\partial \sigma_q(i)} = \frac{2\Delta_r^2}{\sigma_q^3(i)} \sum_{b=0}^{B-1} b^3 \, |A_{\mathrm{p}}(n;\, b, q)|^2 \, \exp\left(-\frac{b^2 \Delta_r^2}{\sigma_q^2(i)}\right). \tag{25}$$

The Step operation translates the estimate $\underline{\sigma}(i)$ in the direction of the gradient (the direction of increasing performance measure) to the vector $\underline{\tilde{\sigma}}(i)$. As a spread vector, $\underline{\tilde{\sigma}}(i)$ corresponds to a radially Gaussian kernel whose volume exceeds the value α. Therefore, in the Project operation, we rescale $\underline{\tilde{\sigma}}(i)$. This rescaling changes the volume, but not the basic shape, of the kernel corresponding to $\underline{\tilde{\sigma}}(i)$. A simple procedure for selecting the iteration step size $\mu(i)$ to ensure a stable algorithm is detailed in [7, 8]. An alternative procedure, the one we use here, grows the kernel volume by a fixed amount, such as a factor of two, in each Step operation. We have found this procedure works well and converges quickly.

In principle, the kernel optimization problem (6)–(8) must be solved at each time point t, at a cost of $O(IM^2)$ computations per time point for M angle and M radius samples in the polar-coordinate STAF and I iterations of the step-project algorithm. However, since the STAF changes only slightly from one time sample to the next, only one or two gradient steps need be taken each time increment to track the optimal kernel over time, reducing the cost to $O(M^2)$ operations per time point.

4.4 AOK TFR time-slice computation

The current-time slice of the AOK TFR is computed as the two-dimensional Fourier transform of the product of the symmetrical STAF and the kernel, both evaluated at time t. For discrete-time data, a two-dimensional fast Fourier transform (FFT) is applied. Since only a single time-slice is required at time n, a full row-column FFT is not needed; instead, we require only

$$\begin{aligned} P_{\mathrm{AOK}}(n,k) &= \sum_m \sum_p A_{\mathrm{d}}(n;p,m)\, \Phi_{\mathrm{opt}}(n;p,m)\, e^{-j2\pi mk/M} \; e^{-j2\pi pn/M} \\ &= \sum_m \sum_p e^{j2\pi p(T-n-m/2)/M} \; \tilde{A}_{\mathrm{d}}(n+T; 2\pi p/M, m)\, \Phi_{\mathrm{opt}}(n;p,m) \\ &\qquad \cdot e^{-j2\pi mk/M} \; e^{-j2\pi pn/M} \\ &= \sum_m \left[\sum_p e^{j2\pi p(T-m/2)/M} \; \tilde{A}_{\mathrm{d}}(n+T; 2\pi p/M, m)\, \Phi_{\mathrm{opt}}(n;p,m) \right] \\ &\qquad \cdot e^{-j2\pi mk/M}. \end{aligned} \tag{26}$$

For a single time n, the inner sum requires M row accumulations (cost $O(M^2)$). A single column FFT (in m) suffices to compute the single-time output slice.

Discretization raises questions related to the necessary sampling rate. We show in Appendix B that sampling the signal at the Nyquist rate is sufficient to prevent aliasing with the AOK algorithm.

4.5 Computational cost

The tricks described in Sections 4.1–4.4 greatly reduce the costs of all components of the AOK TFR algorithm compared to a straightforward implementation. Assuming that M samples are utilized in each of the variables τ, θ, r, and ψ, as is generally the case [7], the overall computational cost per signal sample is $O(M^2)$, as opposed to $O(M^2 \log M)$ for direct application of the algorithm.

When the polar-coordinate STAF is obtained by interpolation, this interpolation, the update of the optimal kernel parameters, and the computation of the output time slice need only be performed when an output time-slice is desired, rather than for each signal sample; this greatly reduces the overall computation when the AOK TFR is decimated in time. However, the recursive nature of the rectangular STAF update requires an $O(M^2)$ computation with each input sample, regardless of whether an output is desired. If the time increment between output TFR slices exceeds $O(\log M)$, it becomes more efficient to compute the STAF in the traditional block fashion using FFTs. Then, the running algorithm reverts to computation using the block algorithm of [6–8] on (perhaps overlapping) successive blocks of data.

5 Examples

Figure 2(a) from the Introduction illustrates the superior performance of the AOK TFR on the synthetic test signal (40). Since this TFR adapts its radially Gaussian kernel to each set of signal components, it yields a highly concentrated, readable representation without the auto-component distortion and cross-components that are apparent in all the representations of Figure 1.

Figure 4 presents contour plots of two fixed-window spectrograms, with, respectively, 64-sample and 128-sample Hamming windows, and the AOK TFR with $\alpha = 4$ of a portion of the bird song of a Cerulean Warbler (*Dendroica cerulea*) [23] sampled at a 16 kHz rate. The AOK TFR is much more concentrated than either spectrogram in all portions of the song, and it resolves the fine structure of the latter, "buzzy," portion of the song much better than the spectrogram with a long window. This data illustrates the benefits of time adaptivity of the kernel, since neither fixed-window spectrogram works well for all portions of the signal.

In Figure 5, we display several TFRs of a synthetic rendering of the French word *caillou* (pronounced "kayu").[5] Unlike the fixed kernel TFRs, the AOK TFRs perform well on all parts of the signal. (We will introduce the cone AOK in Section 6.2.)

[5] Prepared by G. Feng of the Institut de la Communication Parlée, INPG/Université de Grenoble for the Groupement de Recherche CNRS Traitement du Signal et Images.

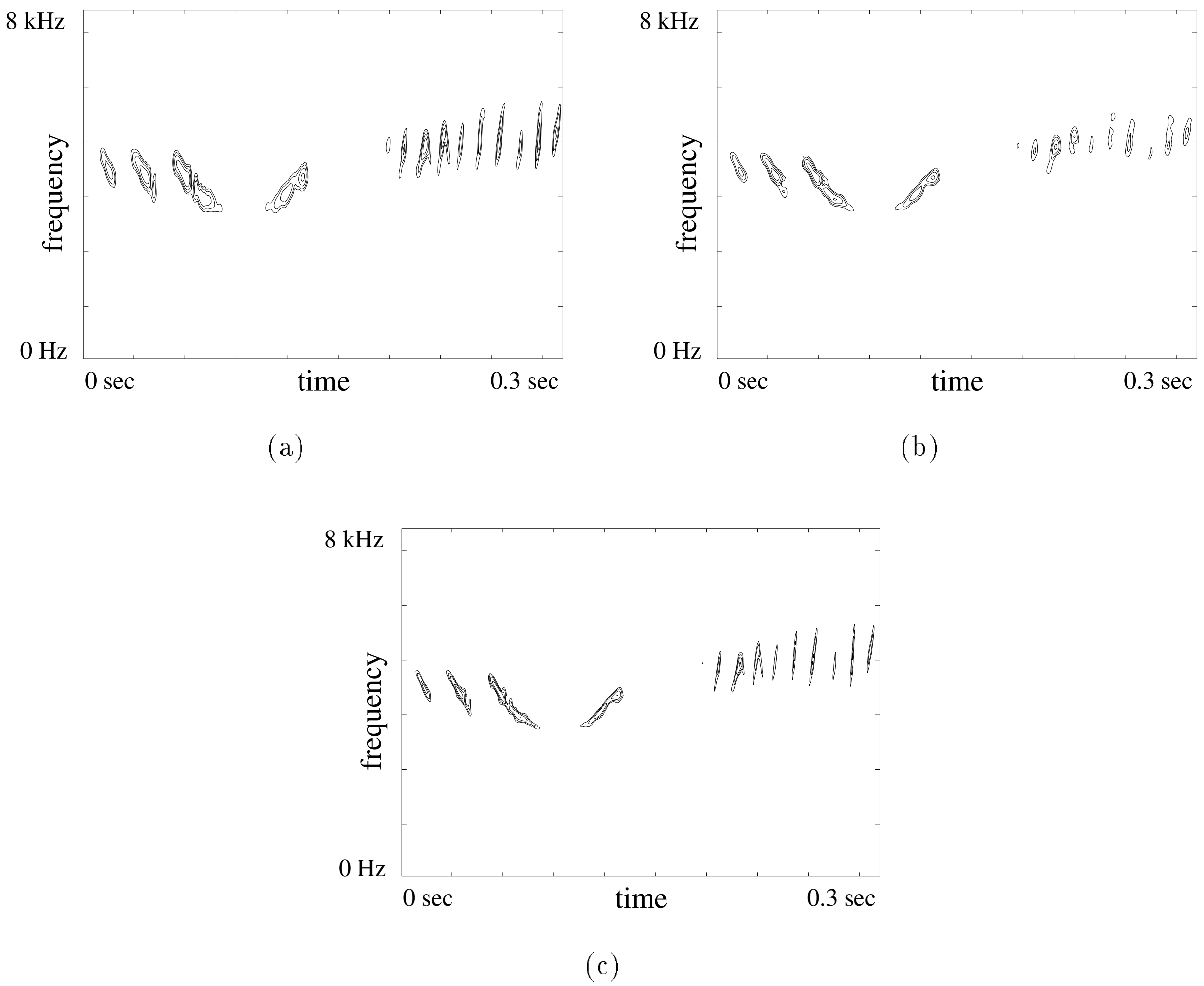

Figure 4: *Comparison of several TFRs of a portion of the bird song of a Cerulean Warbler (Dendroica cerulea)* [23]. *The sample rate was 16 kHz. (a) Spectrogram computed using a short (64-sample) Hamming window. (b) Spectrogram computed using a long (128-sample) Hamming window. (c) AOK TFR of volume* $\alpha = 4$.

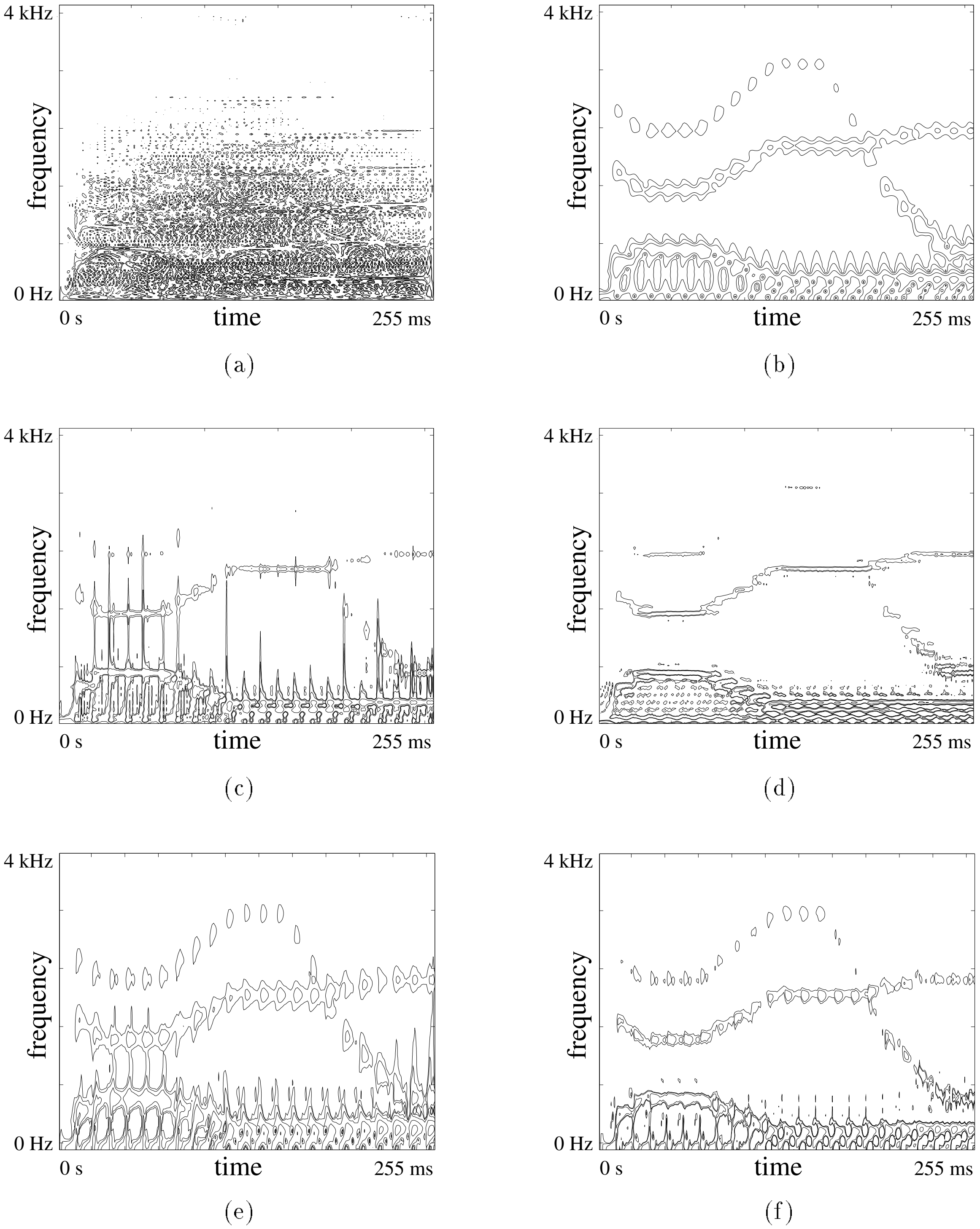

Figure 5: *Comparison of several TFRs of a synthetic speech signal (the word* caillou *from the French). (a) Wigner distribution. (b) Spectrogram. (c) Choi-Williams distribution with smoothing parameter* $\sigma = 1$ [2]*. (d) Cone-kernel representation with* τ*-extent parameter* $= 33$ [3]*. (e) AOK TFR of volume* $\alpha = 1$ *and window width* $2T = 64$*. (f) Cone AOK TFR of volume* $\alpha = 0.3$ *and window width* $2T = 64$*.*

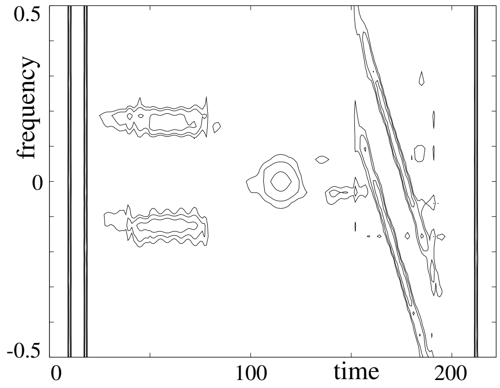

Figure 6: *AOK TFR constrained to preserve marginal distributions applied to the synthetic test signal (40) from Appendix A. Parameters: volume $\alpha = 1.4$, window width $2T = 32$.*

6 Extensions

Extensions of the AOK TFR to incorporate desired constraints or *a priori* knowledge, such as time-support (cone) constraints or approximate preservation of marginals, are often easily implementable with no additional computation. A factor of two in computational savings can be obtained by specializing the algorithm for real-valued signals. We show how to obtain much greater savings when the auto-components are restricted to certain portions of the AF plane, such as for signals without significant chirp components. In this case, the computational expense reduces to the same order as fixed-kernel representations.

6.1 Marginal distribution preservation

Conditions on both continuous [1,2] and discrete [24] kernels for preserving time and/or frequency marginals in a TFR have been developed. These conditions essentially require that

$$\Phi(\theta, 0) \;=\; \Phi(0, \tau) \;=\; 1 \qquad \forall\; \tau, \theta. \tag{27}$$

These constraints can easily be enforced in the kernel design procedure by not adapting the kernel along these two axes. This requires no additional computation. However, since an STAF is used to compute the AOK TFR, only the time marginal is exactly preserved; the frequency marginal is only approximately retained.

Figure 6 illustrates the marginal-preserving AOK TFR on the synthetic test signal (40). The cross-shaped footprint typical of marginal-preserving TFRs is evident.

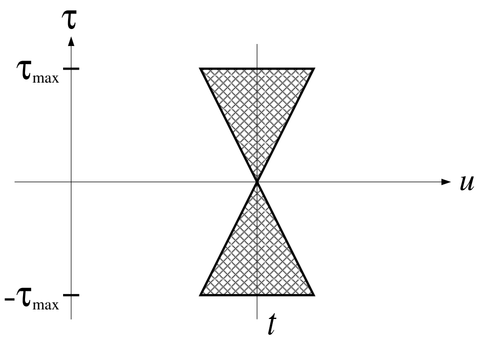

Figure 7: *Region of support in the (u, τ) instantaneous correlation plane for a two-dimensional window $W(u-t, \tau)$ satisfying time-support (cone) constraint (31).*

6.2 Time support preservation

Time-support (cone-kernel) constraints, first introduced in [25] and examined in more detail in [3], have proven to be of considerable value in many applications. These constraints cause the TFR to be zero for all times outside the convex hull of the time support, $\mathcal{C}_s$, of the signal; that is,

$$P(t, \omega) \;=\; 0 \qquad \forall\, t \notin \mathcal{C}_s, \tag{28}$$

with

$$\mathcal{C}_s \;\equiv\; \{t\colon\; s(u) = 0,\; \forall\; u < t \text{ or } u > t\}\,. \tag{29}$$

Cone constraints can be easily implemented in the AOK TFR by utilizing the following windowed STAF

$$A_W(t;\theta,\tau) \;\equiv\; \int s^*\left(u - \frac{\tau}{2}\right) s\left(u + \frac{\tau}{2}\right) W(u-t,\tau)\, e^{j\theta u}\, du, \tag{30}$$

with $W(v, \tau)$ a two-dimensional window function satisfying the cone constraint

$$W(v,\tau) \;=\; 0, \qquad |v| > \frac{1}{2}\,|\tau|. \tag{31}$$

Figure 7 illustrates the support of the windowed instantaneous correlation

$$s^*\left(u - \frac{\tau}{2}\right) s\left(u + \frac{\tau}{2}\right) W(u-t,\tau). \tag{32}$$

For $t \notin \mathcal{C}_s$, it is readily verified that this expression equals zero: for triples (u, t, τ) such that $W(u-t, \tau) \neq 0$, either $u - \frac{\tau}{2} \notin \mathcal{C}_s$ or $u + \frac{\tau}{2} \notin \mathcal{C}_s$. Hence, for $t \notin \mathcal{C}_s$, $A_W(t; \theta, \tau) = 0$ and a time-frequency slice equal to zero at time t results regardless of the kernel.

For "bowtie" window functions of the form

$$W(v,\tau) \;=\; \begin{cases} 1, & |v| \le \frac{1}{2}|\tau| \le \frac{1}{2}\tau_{\max} \\ 0, & \text{otherwise} \end{cases} \tag{33}$$

(see Figure 7), efficient implementation of the cone STAF follows as in Section 4, except with a τ-dependent window. By making the change of variables $v = t - u - \tau/2$ in (30), we obtain

$$A_W(t;\, \theta, \tau) \;=\; e^{j\theta(t-\tau/2)}\, \widetilde{A}_W(t;\, \theta, \tau), \tag{34}$$

where the causal (for each τ), asymmetric cone STAF is given by

$$\widetilde{A}_W(t;\, \theta, \tau) \;\equiv\; \int_0^{\tau} s^*(t - v - \tau)\; s(t - v)\; e^{-j\theta v}\, dv, \qquad \tau \geq 0. \tag{35}$$

As in Section 4, we discretize the asymmetrical cone STAF for implementation. Again assuming the signals are sufficiently bandlimited, a discrete approximation to the asymmetrical cone STAF is given by

$$\widetilde{A}_{\mathrm{d},W}(n;\theta,k) \;\equiv\; \sum_{p=0}^{k} s^*(n - p - k)\; s(n - p)\; e^{-j\theta p}. \tag{36}$$

For a given θ and k, this has an efficient recursive implementation

$$\begin{aligned} \widetilde{A}_{\mathrm{d},W}(n;\theta,k) \;&=\; e^{-j\theta}\, \widetilde{A}_{\mathrm{d},W}(n-1;\theta,k) \;+\; s(n)\, s^*(n-k) \\ &\quad -\; e^{-j\theta(k+1)}\, s(n-k-1))\, s^*(n-2k-1)); \end{aligned} \tag{37}$$

an unconditionally stable version for long data records follows analogously from (18). A discrete version of the symmetrical STAF is obtained from (34) as

$$A_{\mathrm{d},W}(n;\theta,k) \;=\; e^{j\theta(n-k/2)}\, \widetilde{A}_{\mathrm{d},W}(n;\theta,k). \tag{38}$$

Note the great similarity between this algorithm and that for computing the standard STAF; the sum bounds and associated phase factors simply change slightly to accommodate the different support region.

With a fast, recursive algorithm for implementing the cone STAF, the remainder of the efficient algorithm developed in Section 4 now applies without modification. The optimal kernel can be obtained from either the cone STAF or the standard STAF. (We have experimented with both possibilities and have much preferred the latter.) In either case, the optimal kernel is multiplied by the cone STAF to construct the time-support preserving AOK TFR. (Our formulation effectively applies the cone constraints *a posteriori*.) The total computational cost of the algorithm grows slightly compared to the standard method, because both the standard STAF and the cone STAF must be computed, but the difference is minor.

Figure 2(b) illustrates the performance of the cone AOK TFR on the synthetic test signal of (40). The sharper transitions at abrupt signal discontinuities, typical of cone-kernel TFRs, are readily apparent. Similarly, the cone AOK of Figure 5(f) outperforms both the fixed-kernel TFRs and the original flavor AOK TFR on the synthetic speech signal.[6] The cone AOK TFR of the bird chirp data very closely resembles the standard AOK TFR from Figure 4.

[6]Since the cone truncation in (v, τ) coordinates swells the effective volume of the kernel significantly in (θ, τ) coordinates, we compensate with a smaller starting volume (in Figure 5(f), $\alpha = 0.3$).

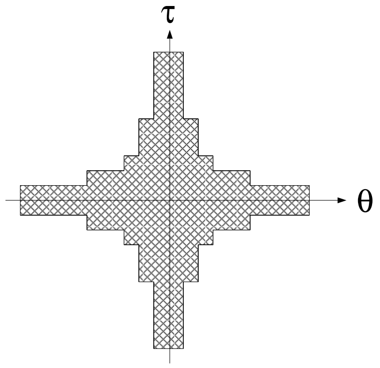

Figure 8: *Region of the (θ, τ) ambiguity plane containing significant auto-component energy for signals without substantial frequency modulation. Only these portions of the STAF need be computed or stored.*

6.3 Real-valued signals

In addition to the symmetry of (20), the STAF of a real-valued signal exhibits the additional symmetry

$$A(t;\, \theta, \tau) = A^*(t;\, -\theta, \tau). \tag{39}$$

Thus the negative θ samples are known by symmetry and need neither be computed nor stored. Exploitation of this symmetry results in a factor of two savings in the computational cost of the algorithm for real-valued signals.

6.4 Reduced STAF Computation

Should it be known *a priori* that portions of the STAF ambiguity plane contain no significant auto-component energy, we desire the kernel to also equal zero in these regions. Neither the kernel nor the AF need be computed or stored at such locations. Since the computational cost of the algorithm is proportional to the number of STAF sample points that must be computed, great savings result when significant portions of the STAF are eliminated.

In particular, for signals without significant frequency modulation (chirp), the auto-component energy will be concentrated along the τ or θ axes, and only relatively narrow strips of the STAF along these axes need be computed. Figure 8 illustrates such a pattern. For strips of width $O(\log M)$ or less, the computational complexity of the algorithm drops from $O(M^2)$ to $O(M \log M)$ per signal sample, which is equivalent to that of fixed-kernel TFRs.

7 Conclusions

While signal-dependent TFRs offers good performance for a large class of signals, adaptation of the kernel over time to track signal variations provides even better performance, as illustrated by the results presented here. A time-adaptive algorithm requires time localization of the signal characteristics, obtained here by a short-time ambiguity function. Efficient implementation of the time-adaptive radially Gaussian kernel TFR requires several algorithmic tricks to reduce the computational cost to $O(NM^2)$, with N the signal length in samples and M the number of frequency samples produced at each time. This exceeds the $O(NM \log M)$ cost of most fixed-kernel TFRs, but the benefits of adaptivity may often outweigh the additional cost.

Certain constraints, such as marginal and outer time support (cone) constraints, can easily be incorporated into the AOK algorithm at little or no additional computational complexity. The cost can even be greatly reduced if the signal components are known *a priori* to be restricted to limited regions of the time-frequency plane. The proposed implementation supports efficient, on-line adaptation of the kernel and running computation of the AOK TFR, thus extending the benefits of adaptive time-frequency representation to real-time applications and signals of arbitrary length.

The AOK TFR represents the high end, in both performance and cost, of adaptive time-frequency analysis methods. Techniques with more limited adaptation that require less computation exist [26,27]; however, their ability to match complicated signals, particularly those with significant frequency modulation, is correspondingly reduced. The preferred method depends on the characteristics of the signal to be analyzed, the required performance, and the computational limitations. In many cases we have found the execution time of the AOK algorithm to be input/output-limited rather than compute-limited on typical workstations.

A C-language program implementing the AOK algorithm is available from the authors.[7]

A Synthetic Test Signal

The test signal utilized in Figures 1 and 2 consists of three impulses, two simultaneous sinusoidal pulses, a Gaussian pulse, and two parallel linear chirps:

$$\begin{aligned} s[n] \;=\;& 6\,\delta[n-11] \;+\; 6\,\delta[n-19] \;+\; r_{40,79}[n]\left[e^{-j\frac{\pi}{6}(n-39)} \;+\; e^{j\frac{\pi}{8}(n-39)}\right] \\ &+\; 1.41\, r_{90,142}[n]\, e^{-(n-116)^2/100} \\ &+\; r_{153,192}[n]\, e^{-j0.03(n-152)^2}\left[e^{-j\frac{\pi}{2}(n-152)} \;+\; e^{-j\frac{\pi}{5}(n-152)}\right] \\ &+\; 6\,\delta[n-213], \end{aligned} \tag{40}$$

with $r_{a,b}[n]$ the gating function

$$r_{a,b}[n] \;=\; \begin{cases} 1, & a \le n \le b \\ 0, & \text{otherwise.} \end{cases} \tag{41}$$

[7]Email: `d-jones@csl.uiuc.edu` and `richb@rice.edu`.

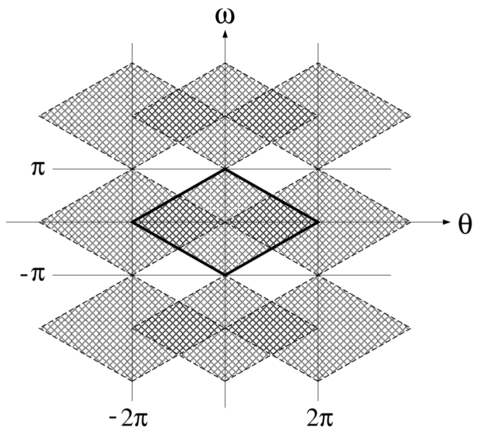

Figure 9: *The region of support in (θ, ω) of the spectral correlation function (42) of a signal bandlimited to π rad/sec (solid boundary), and the two-dimensional spectral aliasing induced by Nyquist 2π rad/sec sampling of the signal. Note that no aliased terms appear along the $\theta = 0$ axis, which is the only portion of this plane used to compute the AOK TFR.*

B Sampling Issues

As shown by Nuttall [19] and later by Jeong and Williams [20], the support of the spectral correlation function

$$\widehat{R}(\theta, \omega) \;\equiv\; S^*\!\left(\omega - \frac{\theta}{2}\right) S^*\!\left(\omega + \frac{\theta}{2}\right) \tag{42}$$

of a signal bandlimited to π rad/sec is limited to a diamond-shaped region between $\pm\pi$ rad/sec in ω and $\pm 2\pi$ rad/sec in θ, as illustrated in Figure 9. (Here, $S(\omega)$ denotes the Fourier transform of the signal $s(t)$.) This implies that unit-time sampling in τ suffices to avoid aliasing in ω in time-frequency. However, unit-time sampling in the dependent (t) variable in computing the AF is insufficient to prevent aliasing of high θ frequencies, which could lead to aliasing artifacts in the time variable t in time-frequency. The dashed diamonds in Figure 9 illustrate the spectral copies induced by unit-time sampling of the signal.

At first glance, this aliasing problem appears to necessitate oversampling of the signal. However, recall that, at each time, only a single time-slice of the AOK TFR is computed. Fortuitously, for the time-slice corresponding to the center of the window, no aliasing artifacts can occur with a strictly bandlimited signal.

To demonstrate this, recall from (11) that the AOK TFR is the two-dimensional Fourier transform of the STAF-kernel product. Thus, using (10) and making the change of variable $u = v + t$, we have

$$\begin{aligned} P_{\mathrm{AOK}}(t, \omega) &= \frac{1}{4\pi^2} \iint A(t;\, \theta, \tau)\, \Phi_{\mathrm{opt}}(t; \theta, \tau)\, e^{-j\omega\tau - j\theta t}\, d\theta\, d\tau \\ &= \frac{1}{4\pi^2} \iiint s^*\!\left(v + t - \frac{\tau}{2}\right)\, w^*\!\left(v - \frac{\tau}{2}\right) \end{aligned}$$

$$\cdot\, s\Big(v+t+\frac{\tau}{2}\Big)\; w\Big(v+\frac{\tau}{2}\Big)\; e^{j\theta v}\, dv\;\; \Phi_{\mathrm{opt}}(t;\,\theta,\tau)\, e^{-j\omega\tau}\, d\theta\, d\tau. \tag{43}$$

Thus only the $\theta = 0$ axis of the spectral correlation function, which for strictly bandlimited signals contains no aliased components, is included in the current-time TFR slice, and therefore no aliasing occurs.

Nuttall points out in [19] that a minimum of half-sample spacing in the time variable is necessary for accurate representation of the TFR of a Nyquist-sampled signal. The procedure proposed here produces time slices at unit-sample spacing and thus undersamples the TFR in the t direction (although for most applications this is acceptable); however, it avoids any other aliasing artifacts. Should half-sample spacing be desired, it can easily be obtained by introducing a phase-shift corresponding to a half-sample advance or delay in (26)

$$P_{\mathrm{AOK}}\Big(n\pm\frac{1}{2},k\Big) \;=\; \sum_m \Big[\sum_p e^{j2\pi p(T\mp 1/2-m/2)/M}\; \Phi_n(m,p)\, \widetilde{A}_{\mathrm{d}}(n+T;2\pi p/M,m)\Big]\; e^{-j2\pi mk/M}. \tag{44}$$

Acknowledgments

The authors wish to express their thanks to Tom Pollard and Wade Bastien for suggesting improvements to the code implementing the AOK TFR, and to Tom Brotherton for naming and testing the algorithm. The authors also thank G. Feng of the Institut de la Communication Parlée, INPG/Université de Grenoble, for the synthetic speech data. This data was prepared by the Groupement de Recherche CNRS Traitement du Signal et Images for its Signaux Test managed by Patrick Flandrin.

This work was sponsored by the National Science Foundation, grant nos. MIP 9012747 and MIP 9457438, the Joint Services Electronics Program, grant no. N00014-90-J-1270, the Texas Advanced Technology Program, grant no. TX-ATP 003604–002, and the Sound Group of the Computer-based Education Research Laboratory at the University of Illinois.

References

[1] L. Cohen, "Time-frequency distributions — A review," *Proc. IEEE*, vol. 77, pp. 941–981, July 1989.

[2] H. I. Choi and W. J. Williams, "Improved time-frequency representation of multicomponent signals using exponential kernels," *IEEE Trans. Acoust., Speech, Signal Processing*, vol. 37, pp. 862–871, June 1989.

[3] Y. Zhao, L. E. Atlas, and R. J. Marks, "The use of cone-shaped kernels for generalized time-frequency representations of nonstationary signals," *IEEE Trans. Acoust., Speech, Signal Processing*, vol. 38, pp. 1084–1091, July 1990.

[4] D. L. Jones and T. W. Parks, "A high resolution data-adaptive time-frequency representation," *IEEE Trans. Acoust., Speech, Signal Processing*, vol. 38, pp. 2127–2135, Dec. 1990.

[5] R. G. Baraniuk and D. L. Jones, "A signal-dependent time-frequency representation: Optimal kernel design," *IEEE Trans. Signal Processing*, vol. 41, pp. 1589–1602, Apr. 1993.

[6] R. G. Baraniuk and D. L. Jones, "A radially Gaussian, signal-dependent time-frequency representation," in *Proc. IEEE Int. Conf. Acoust., Speech, Signal Processing — ICASSP '91*, pp. 3181–3184, 1991.

[7] R. G. Baraniuk, "Shear madness: Signal-dependent and metaplectic time-frequency representations," tech. rep., no. UILU–ENG–92–2226, Coord. Sci. Lab., Univ. Illinois, Urbana-Champaign, 1992.

[8] R. G. Baraniuk and D. L. Jones, "A radially Gaussian, signal-dependent time-frequency representation," *Signal Processing*, vol. 32, pp. 263–284, June 1993.

[9] R. G. Baraniuk and D. L. Jones, "A signal-dependent time-frequency representation: Fast algorithm for optimal kernel design," *IEEE Trans. Signal Processing*, vol. 42, pp. 134–146, Jan. 1994.

[10] D. L. Jones and R. G. Baraniuk, "An on-line signal-dependent time-frequency representation," in *Fifth IEEE Digital Signal Processing Workshop*, (Starved Rock Lodge, IL), Sept. 1992.

[11] D. L. Jones and R. G. Baraniuk, "An adaptive optimal kernel time-frequency representation," in *Proc. IEEE Int. Conf. Acoust., Speech, Signal Processing — ICASSP '93*, 1993.

[12] P. Flandrin, "Some features of time-frequency representations of multicomponent signals," in *Proc. IEEE Int. Conf. Acoust., Speech, Signal Processing — ICASSP '84*, pp. 41.B.4.1–41.B.4.4, 1984.

[13] J. G. Proakis and D. G. Manolakis, *Introduction to Digital Signal Processing.* New York: Macmillan, 1988.

[14] M. Unser, "Recursion in short-time signal analysis," *Signal Processing*, vol. 5, pp. 229–240, May 1983.

[15] M. G. Amin, "Time-frequency spectrum analysis and estimation for non-stationalry random processes," in *Time-Frequency Signal Analysis — Methods and Applications* (B. Boashash, ed.), pp. 208–232, Melbourne: Longman Cheshire, 1992.

[16] M. G. Amin, "Recursion in Wigner distribution," in *Proc. SPIE Int. Soc. Opt. Eng.*, vol. 975, pp. 221–231, 1988.

[17] M. G. Amin, "Computationally lag-invariant recursive spectrum estimators," *IEEE Trans. Acoust., Speech, Signal Processing*, vol. 35, pp. 1713–1724, Dec. 1987.

[18] M. G. Amin, "Order-recursive spectrum estimation," *Proc. IEEE*, vol. 76, pp. 289–290, Mar. 1988.

[19] A. H. Nuttall, "Alias-free Wigner distribution function and complex ambiguity function for discrete signals," Tech. Rep. NUSC 8533, Naval Underwater Syst. Cntr., Apr. 1989.

[20] J. Jeong and W. J. Williams, "Alias-free generalized discrete-time time-frequency distributions," *IEEE Trans. Signal Processing*, vol. 40, pp. 2757–2765, Nov. 1992.

[21] J. R. O'Hair and B. W. Suter, "Kernel design techniques for alias-free time-frequency distributions," in *Proc. IEEE Int. Conf. Acoust., Speech, Signal Processing — ICASSP '94*, vol. III, pp. 333–336, 1994.

[22] D. Wu and J. M. Morris, "Discrete Cohen's class of distributions," *IEEE Int. Symp. Time-Frequency and Time-Scale Analysis*, pp. 532–535, Oct. 1994.

[23] D. J. Boorer, *Common Bird Songs (Audio Cassette)*. New York: Dover, 1984.

[24] B. Boashash, "Time-Frequency Signal Analysis," in *Advances in Spectrum Estimation and Array Processing*, S. Haykin, Ed. Englewood Cliffs, NJ: Prentice-Hall, 1991, vol. 1, pp. 418–517.

[25] T. A. C. M. Claasen and W. F. G. Mecklenbräuker, "The Wigner distribution — A tool for time-frequency signal analysis — Part I: Continuous-time signals," *Philips J. Res.*, vol. 35, no. 3, pp. 217–250, 1980.

[26] D. L. Jones and R. G. Baraniuk, "A simple scheme for adapting time-frequency representations," *IEEE Trans. Signal Processing*, vol. 42, pp. 3530–3535, Dec. 1994.

[27] R. N. Czerwinski and D. L. Jones, "An adaptive time-frequency representation using a cone-shaped kernel," in *Proc. IEEE Int. Conf. Acoust., Speech, Signal Processing — ICASSP '93*, vol. IV, pp. 104–107, 1993.

Figure Captions